8-15-2009

Thermionic emission energy distribution from nanocrystalline diamond films for direct thermal-electrical energy conversion applications

Kishore Uppireddi
University of Puerto Rico

Tyler Westover
Purdue University - Main Campus, twestove@purdue.edu

Timothy Fisher
Purdue University - Main Campus, tsfisher@purdue.edu

Brad H. Weiner
University of Puerto Rico

Gerardo Morell
University of Puerto Rico

Thermionic emission energy distribution from nanocrystalline diamond films for direct thermal-electrical energy conversion applications

Kishore Uppireddi,[1,4,a)] Tyler L. Westover,[4] Timothy S. Fisher,[4] Brad R. Weiner,[1,3] and Gerardo Morell[1,2]
[1]*Institute for Functional Nanomaterials, University of Puerto Rico, San Juan, Puerto Rico 00931, USA*
[2]*Department of Physics, University of Puerto Rico, San Juan, Puerto Rico 00931, USA*
[3]*Department of Chemistry, University of Puerto Rico, San Juan, Puerto Rico 00931, USA*
[4]*Birck Nanotechnology Center, Purdue University, West Lafayette, Indiana 47907, USA*

(Received 29 May 2009; accepted 18 July 2009; published online 28 August 2009)

In the ongoing quest for energy production by nonconventional methods, energy conversion by vacuum and solid-state thermionic emission devices is one of the potentially efficient pathways for converting thermal energy directly into electrical power. The realization of practical of thermionic energy conversion devices strongly depends on achieving low work function materials, which is thus far a limiting factor. In an attempt to develop a new low work function thermionic material, this work reports thermionic emission energy distributions (TEEDs) from nanocrystalline diamond (NCD) films in the temperature range from 700 to 900 °C that reveal a consistent effective work function of 3.3 eV. The NCD films also exhibit emission peaks corresponding to higher work functions as indicated by shifts in their energy position and relative intensity as a function of temperature. These shifts thus appear to be related to instabilities in the NCD's surface chemistry. The analysis of these data yields information on the origin of the low effective work function of NCD. © *2009 American Institute of Physics*. [DOI: 10.1063/1.3204667]

I. INTRODUCTION

Direct thermal-to-electrical energy conversion systems that can operate at moderate temperatures (300–650 °C) with high efficiencies provide the possibility of harnessing thermionic power conversion and for waste heat recovery applications.[1–4] Both vacuum and solid-state thermionic emission offer potential pathways for generating electrical power from heat. Conventional vacuum thermionic emission conversion (VTEC) is based on the ejection of high-energy electrons from a hot surface upon surmounting the surface potential energy barrier (i.e., work function) and their collection at a cooler surface which is separated by a narrow vacuum gap. The vacuum gap in VTEC devices helps in the reduction of heat losses by conduction. The unique advantages of this technology are compactness, scalability, and high waste rejection temperatures for cascading systems.[5,6] However, the realization of efficient power generation by thermionic emission requires the development of low work function materials. The primary limitations in the applicability of thermionic power generation by thermionic emitter materials are associated with the high operating temperatures needed to produce sufficient electron emission from high work function materials.

Some of earliest and most significant studies on thermionic emission from chemical vapor deposited (CVD) micro- and nanocrystalline diamond (NCD) were done by the Koeck *et al.*,[7] Garguilo *et al.*,[8] Robinson and co-workers,[9,10] and Westover *et al.*[11] Koeck *et al.*[7] studied the field-assisted thermionic emission from nitrogen and sulfur-doped CVD NCD films and estimated an effective work function of 1.5–1.9 eV for nitrogen-doped films and approximately 2.5 eV for sulfur-doped films by fitting experimental data with Richardson–Dushman equation.[12,13] These studies focused on field-assisted thermionic emission, while the present work addresses the electron energy distribution of unassisted thermionic emission from NCD. Detailed studies on the effect of adsorbates on the thermionic emission energy distribution (TEED) were reported by Robinson *et al.*[3] on B-doped NCD films, and work functions as low as 3.95 and 3.88 eV were measured for hydrogen- and nitrophenyl-terminated films, respectively. By regenerating the hydrogen termination on the NCD films, they were able to reproduce the original behavior; however the nonuniformity in the emitter work function limited the practicality of the material for device applications.

NCD is an emerging technological material with electronics and biological applications.[14–17] In an attempt to achieve thermionic emission from NCD films at lower temperatures and without the requirement of chemical adsorbates or doping, we studied the TEED spectra of NCD films that are relatively rich in mid gap states[18] using Ar-rich hot filament chemical vapor deposition (HFCVD) with positive substrate bias.

II. EXPERIMENTAL DETAILS

The NCD films were deposited using a custom-built HFCVD system. The schematics of the chamber with biasing configuration and the details on the deposition parameters are described elsewhere.[19–21] Briefly, the NCD films used in this study were deposited at a gas volume fraction of $CH_4/(CH_4+H_2)=2.54\%$ and $Ar/(Ar+H_2)=80\%$ and at a nominal substrate temperature of 800, 600, and 400 °C. The

a)Electronic mail: uppireddi@gmail.com.

films were deposited on polished molybdenum substrates under positive bias (200 V DC) at constant current of 25 mA with a filament temperature close to 2400 °C. They are hereafter identified as s@800, s@600, and s@400 throughout this article. The surface morphology of the films was investigated by Scanning Electron Microscopy (SEM) using a JEOL JSM 845A Model microscope.

The TEED spectra were measured with a hemispherical energy analyzer (SPECS-Phoibos 100 SCD) connected to a vacuum chamber that achieves pressure on the order of 10^{-8} Torr as described previously.[3,11] Based on free-electron theory, the TEEDs are described by[22]

$$\frac{dJ}{dE} = \frac{4\pi mq}{\hbar^3} \frac{E-\phi}{1+\exp\left(\frac{E-\phi}{k_B T}\right)} H(E-\phi), \tag{1}$$

where J is the saturation current density, m is electron mass, q is charge of the electron, $\hbar$ is the reduced Planck's constant, k_B is Boltzmann's constant, T is the temperature of the surface, and ϕ is the emitter work function. The energy distribution of electrons in the emitter is governed by the Fermi–Dirac function as prescribed by Eq. (1). Importantly, only electrons with kinetic energies greater than the material's work function are eligible for emission as represented by the Heaviside step function $H(E-\phi)$. The maximum thermionic emission intensity predicted by Eq. (1) occurs at an energy $E=\phi+k_BT$. Thus, by comparing the theoretical energy distribution with that obtained from experiments, Eq. (1) can be conveniently used to estimate the work function of a material. Due to finite instrument resolution, measured TEEDs consists of a convolution of the theoretical electron energy distribution and a Gaussian instrument spreading function G_I, which is determined by specific analyzer parameters as[23,24]

$$G_I = \frac{1}{\sigma\sqrt{2\pi}} \exp\left[-\frac{1}{2}\left(\frac{E-E'}{\sigma}\right)^2\right]. \tag{2}$$

The effects of analyzer settings are manifest in the standard deviation σ, referred as the analyzer resolution. The actually measured TEEDs from the analyzer are convolutions of Eqs. (1) and (2).

For a more accurate estimate of work function, the σ term should be small because at higher values of σ the energy peak smears according to the convolution of Eqs. (1) and (2). For proper positioning of TEEDs on the energy axis, the work function of electron detector must be known. The analyzer resolution and detector work function are determined by calibrating the electron analyzer using a free-electron metal sample with a known work function.[25]

The emitter sample under study was located on a 2.54 cm diameter molybdenum substrate heater which is positioned at the analyzer focal plane (i.e., 40 mm below the aperture). The heater assembly was thermally and electrically isolated from other components in the vacuum chamber by alumina hardware. The temperature of molybdenum heater (HeatWave Laboratories, Inc.) was measured using a K-type thermocouple embedded 1 mm below the top surface of the sample and was connected to a proportional temperature controller. An optical pyrometer is used to measure the surface temperature, which differs from the thermocouple temperature due to radiative heat losses between the surface of the sample and the thermocouple and the contact resistance between the heater and sample; the uncertainty in temperature measurements is estimated to be ±30 °C.[26] Electrons emitting from samples were accelerated into the analyzer by grounding the analyzer's nozzle and negatively biasing the heater to a dc power supply (Hewlett Packard 6542A) by a few volts. This small accelerating voltage over the 40 mm vacuum gap is expected to produce no appreciable field emission. Voltage sense lines for the dc power supply were implemented to reduce the uncertainty in the acceleration voltage to ±0.3 mV.

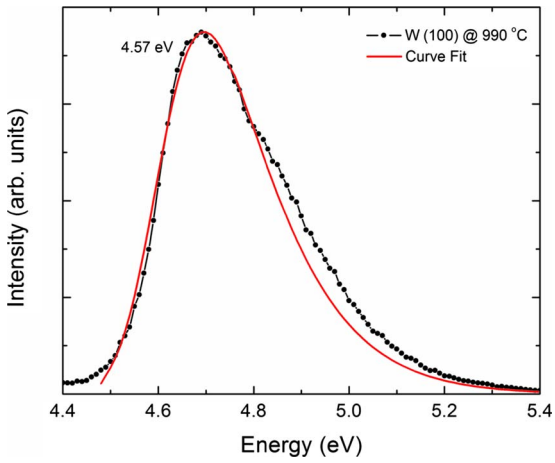

FIG. 1. (Color online) TEED from single crystal tungsten with (100) orientation at 900 °C used to calibrate the experimental set up. The experimental data is represented with dotted line, and the corresponding curve fit obtained by the convolution of Eqs. (1) and (2) (referred as theoretical line) used to estimate the work function is shown with a solid line.

III. RESULTS AND DISCUSSION

The TEED spectra from s@600 and s@400 NCD films at 650/675, 750, 800, 850 and at maximum temperature of 900 °C were recorded. The TEED measurements from s@800 NCD did not produce any substantial thermionic emission over the temperature range; consequently, only the results of s@600 and s@400 NCD films are presented here. Before taking TEED measurements, the instrument was calibrated using single crystalline tungsten (W) with (100) orientation whose work function is well documented, ranging from 4.52–4.59 eV.[27,28] Figure 1 shows the normalized TEED spectra obtained from a W (100) sample at 990 °C along with least square fit line (represented as solid line in the figures referred to as theoretical line) obtained from convolution of Eqs. (1) and (2). The sharp increase in intensity followed by a gently sloping high-energy tail is characteristic the partial occupation of high-energy states according to Fermi–Dirac distribution. The obtained work function 4.57 eV of W (100) is consistent with the literature. Another possible source of thermionic electrons is the molybdenum heater. However, additional experiments show that electron emission from the bare heater surface is only appears at high

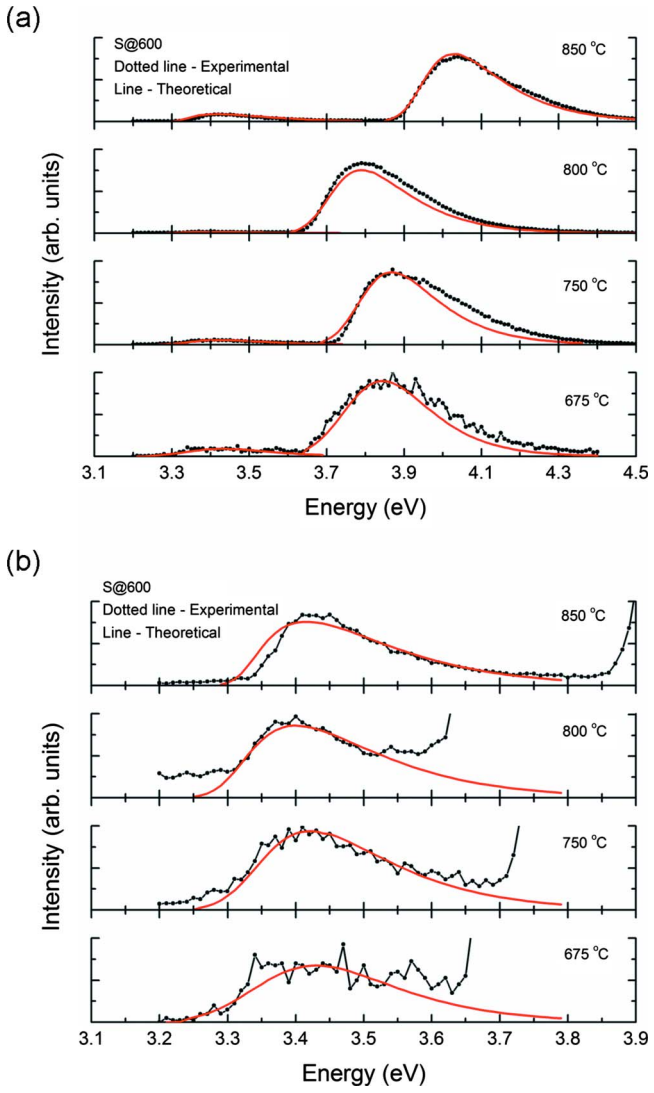

FIG. 2. (Color online) Normalized TEEDs from NCD s@600 NCD measured at 675, 750, 800, and 850 °C with respective theoretical fit lines: (a) for both low and high work function peaks, and (b) the magnified TEED spectrum to reveal the low work function peak at ~3.32 eV.

temperatures (>800 °C), and that the effective work function of the heater surface is 4.4–4.6 eV depending on where analyzer is focused on the heater surface.

Figure 2(a) shows the TEED spectra for s@600 NCD at the specified temperatures, where the experimental data is indicated with dotted line and the corresponding theoretical distribution based on the convolution of Eqs. (1) and (2) is shown with the solid line for each individual peak. The data exhibit two distinct peaks, one at lower energy and other at higher energy, revealing two different regions with different *effective* work functions. The low-energy, low-intensity peak is magnified in Fig. 2(b), and the work functions obtained by curve fitting at the respective temperatures are in Table I. The work function of the surface, in general, is affected by crystal orientation and the presence of impurities and adsorbates [such as dopants, defects, and the negative electron affinity (NEA) effect by hydrogen termination]. It is evident that s@600 NCD shows a consistent low work function around 3.32 eV with relatively much lower intensity than the high-energy dispersive peak, which exhibits a work function range

TABLE I. Summary of the estimated work functions for the corresponding peaks by curve fitting experimental data with that of theoretical equation obtained from the convolution of Eqs. (1) and (2) for the s@600 NCD at respective temperatures.

Temperature of the sample °C	TEED-peak 1 position (eV)	TEED-peak 2 position (eV)
675	3.3	3.72
750	3.32	3.76
800	3.3	3.68
850	3.32	3.92
900	3.34	4.52
850 after reaching 900	3.33	4.51

of 3.72–4.52 eV. If a surface contains areas with distinct work function values, then a TEED can contain multiple peaks whose relative intensity depends on the effective area and work function of each emission site,[3] as seen in our results. In this case, electron emission from the high-energy peak may be originating from an adsorbate state rather than midband-gap state. If the thermionic electron emission originated from an energy state within the band gap, then the intensity (thermionic current) would increase with increasing temperature and, the peak position would not change with increasing temperature.[3] On the other hand, if the TEED spectrum exhibits broadening with a single distinguishable peak, it would be due to moderate work function variation across the surface.

Importantly, the position of low-energy peak did not shift with increasing temperature, as illustrated in Fig. 2(b), indicating that the emission originated from an energy state within the material's band gap. The TEED spectra of s@600 NCD were measured at 850 °C and at the maximum temperature of 900 °C, and again at 850 °C by subsequently reducing temperature, as shown in Fig. 3(a). These measurements were taken due to the fact that surface hydrogen desorption from diamond occurs near 900 °C, consequently leading to positive electron affinity.[25,29,30] Recent studies on CVD micro- and NCD films reported the loss of NEA in the temperature range 700–800 °C.[31,32] The relative intensity of the low-energy peak with a work function near 3.3 eV increased at the maximum temperature of 900 °C as shown in Fig. 3(a). The estimated work function values before and after maximum temperature are summarized in Table I. The consistency of this low-energy peak was tested by keeping the s@600 NCD at 940 °C for 20 min before reducing the temperature to 850 °C. The position of this consistent low work function peak along with curve-fitted data at the respective temperatures is magnified in the Fig. 3(b).

Similar measurements were made on s@400 NCD at 650, 750, 800, 850, 900 and then at 850 °C. Their TEED spectra are shown in Fig. 4(a), and the peak positions are summarized in Table II. This sample also exhibited a consistent peak with an estimated work function around 3.3 eV, which is shown in Fig. 4(b). This low work function peak permanently disappeared when the sample was heated to 900 °C, as shown in Fig. 5. This is probably due to desorption, and is consistent with a drop in vacuum pressure from

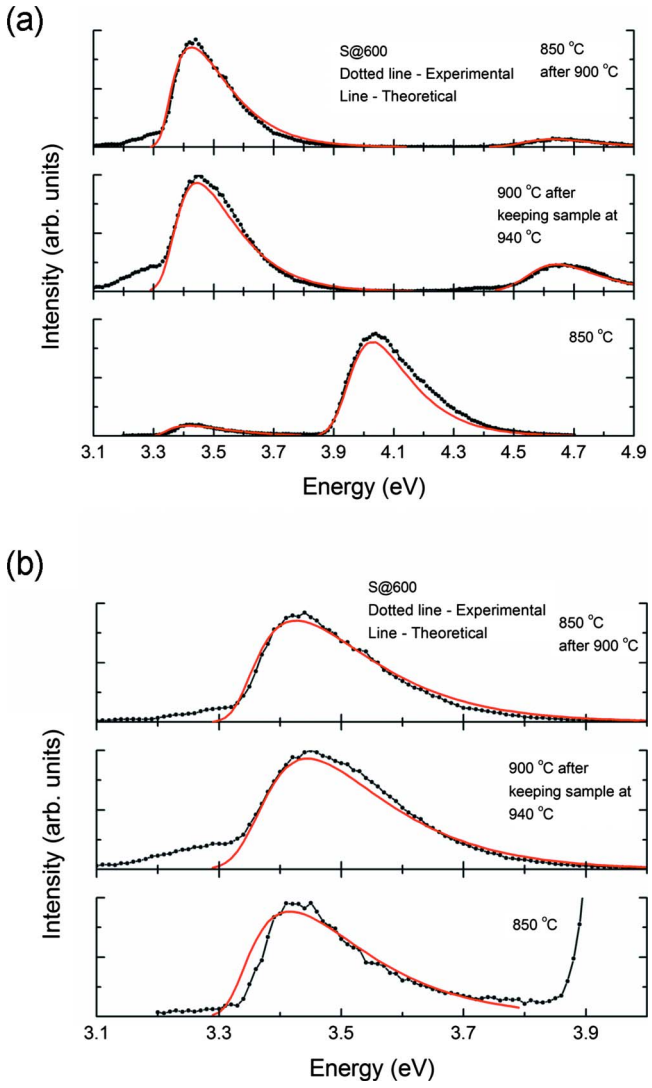

FIG. 3. (Color online) Sequential TEEDs from s@600 NCD measured at 850, 900, and 850 °C along with respective theoretical fit line for estimating the work function: (a) as shown there is sharp increase in the intensity of low work function peak at and after the maximum temperature 900 °C, and (b) with magnified scale to clearly distinguish the sharp rise at ~3.32 eV.

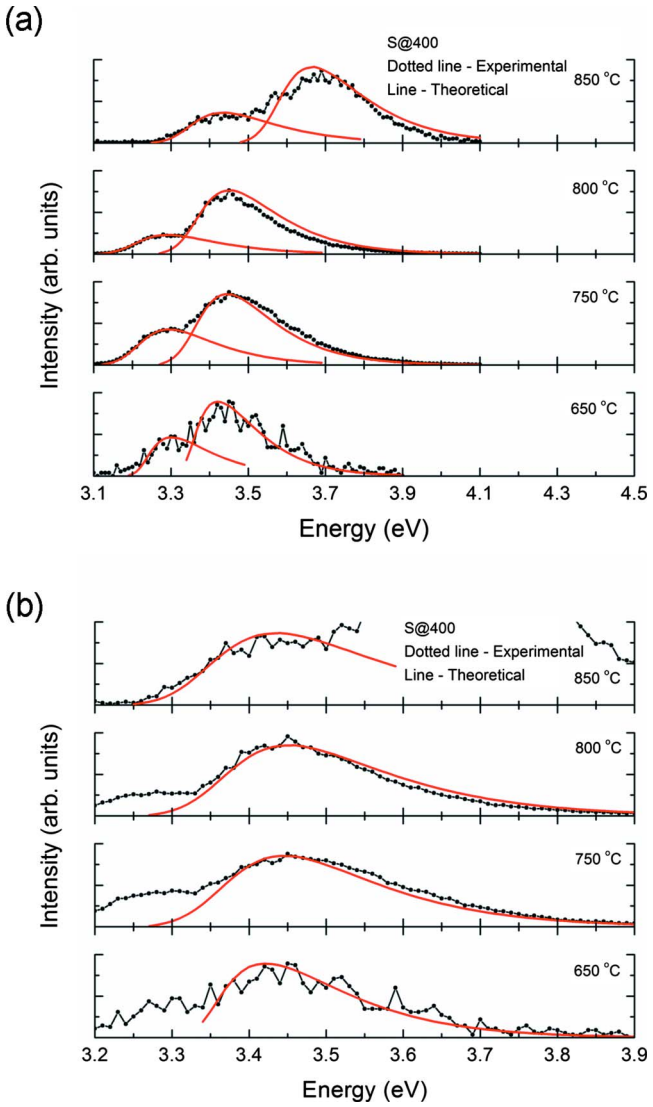

FIG. 4. (Color online) Normalized TEEDs from NCD s@400 measured at 650, 750, 800, and 850 °C with respective theoretical fit lines: (a) for both low and high work function peaks, and (b) the magnified TEED spectrum to reveal the low work function peak at ~3.32 eV.

6×10^{-8} to 9.2×10^{-8} Torr which was observed during this time. However, SEM micrographs of the sample before and after measurements did not reveal major changes in the surface topography, as shown in Fig. 6.

Figure 7 shows the energy level motive diagram for three possible situations that may result in a low work function near 3.3 eV as measured in these films. These situations correspond to NEA, pinning of the Fermi level, and the presence of midband-gap state by either dopants or defects. To elucidate this phenomenon, the values of band gap, position of the Fermi level, and band bending due to charge exchange must be known as well as the magnitude of NEA and positive electron affinity values for the NCD films. It has been shown that NCD films exhibit a band gap of 5.47 eV and that the Fermi level lies 1 ± 0.2 eV (~1 eV) above the valence band.[33] It was also shown that polycrystalline[34,35] CVD diamond films exhibited an effective NEA of −1.1 eV with hydrogen termination. Assuming that the NCD films have (i) an effective NEA of −1.1 eV due to hydrogen termination, ii) small band bending, and (iii) a positive electron affinity of 0.38 eV[35,36] when hydrogen termination is desorbed, we have drawn the motive diagram to point out the source of origin for the low work function peak. We discuss these three scenarios further in the following paragraphs.

TABLE II. Summary of the estimated work functions for the corresponding peaks by curve fitting experimental data with that of theoretical equation obtained from the convolution of Eqs. (1) and (2) for the s@400 NCD at respective temperatures.

Temperature of the sample °C	TEED-peak 1 position (eV)	TEED-peak 2 position (eV)
650	3.22	3.34
750	3.19	3.34
800	3.18	3.34
850	3.32	3.55
900	4.14	4.45
850 after reaching 900	4.14	4.41

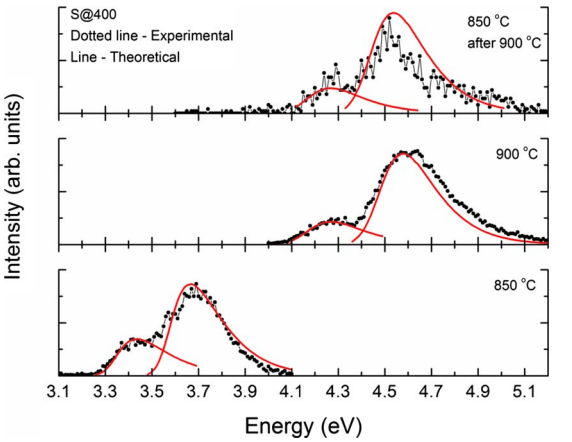

FIG. 5. (Color online) TEEDs from the s@400 NCD measured consecutively at 850, 900, and 850 °C. The film lost the low work function peak at and after the maximum temperature measurement.

When diamond films are terminated with hydrogen (as in CVD diamond films) they can exhibit NEA, which can be expressed as the situation created when the vacuum level (VL) lies below the conduction band minimum (CBM) resulting in an electron affinity value smaller than the surface potential. This modifies the work function value due to the changing position of the VL.[36,37] Figure 7(a) shows the motive energy level band diagram of NCD film with an effective NEA of −1.1 eV and band gap of 5.47. The CBM and valence band maximum have a slight downward band bending due to the *p*-type conductive nature of intrinsic CVD diamond films.[38] This would result in a work function of 3.3 eV by the following equation: Band gap−[NEA+ difference in Fermilevel and valence band including the band bending (η)]. That is $5.47-(1.1+1+\eta)=3.3$ eV with the assumption of band bending value of 0.7 eV. On the other hand, as described above, at sufficiently high temperature (700–800 °C) the samples lose the surface hydrogen, leading to positive electron affinity.[31,32] But the presence of the low work function peak at 3.3 eV and after the maximum temperature measurement of 900 °C [Fig. 2(b)] combined with the loss of hydrogen around 700–800 °C, does not seem to justify NEA for its origin.

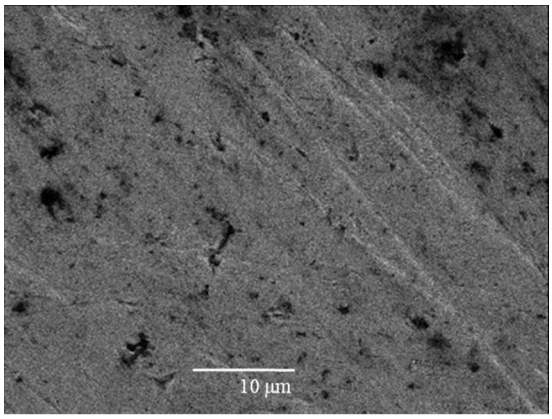

(a)

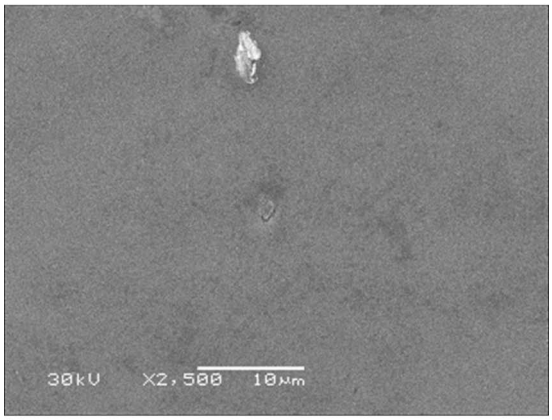

(b)

FIG. 6. SEM micrographs of s@400 NCD (a) before and (b) after the TEEDs acquisition.

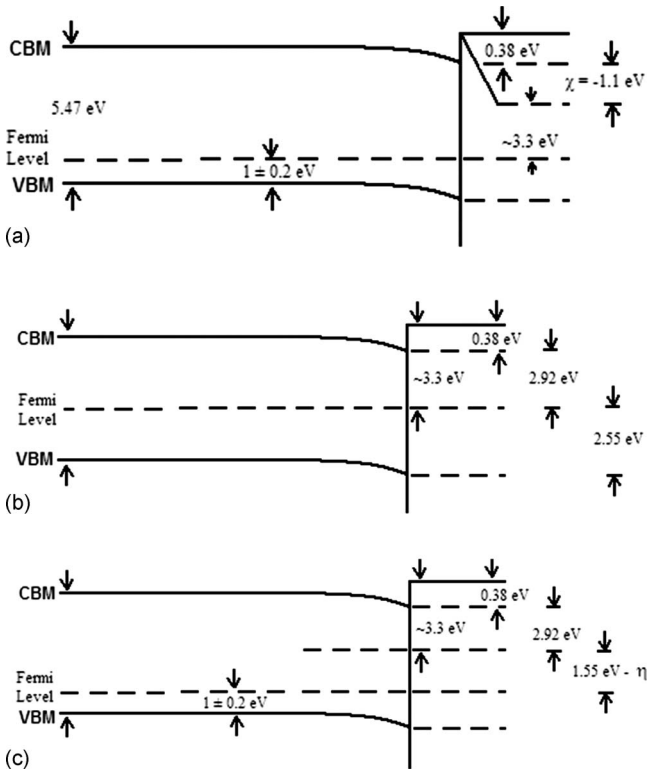

FIG. 7. Motive energy level diagram depicting three possible circumstance leading to a low work function of ~3.3 eV by (a) NEA, (b) pinning of the Fermi level, and (c) midband-gap states.

The other possibility is the pinning of the Fermi level at 3.3 eV below the VL without any NEA effect as shown in Fig. 7(b). Though it is possible, there is no experimental evidence to support this conjecture. Thus we believe that the third situation is most likely; the presence of midband-gap states introduced either by dopants or defects at approximately 3.3 eV below the VL with the assumption of pinning of the Fermi level at ~1 eV above the valence band, without any NEA, as shown in Fig. 7(c). This scenario results in $5.47-(2.92+1+\eta)=(1.55-\eta)$ eV energy difference between the midband-gap state and Fermi level, where η is the band bending.

The midband-gap states could originate from dopants or defects[39] and/or from energy states introduced by nanometer sized grain boundary carbon.[40,41] X-ray photoemission spec-

troscopy (XPS) and Auger measurements (scans not shown) of NCD films did not reveal any appreciable presence of foreign elements, thus ruling out the possibility of dopants and leaving the possibility of energy states introduced either by grain boundary carbon and/or defects. The computational studies done by Keblinski *et al.*[42,43] showed the presence of midband-gap states in diamond due to the existence of disordered carbon with sp^2 and sp^3 bonding at nanometer sized grain boundaries. They also indicated that the size and kind (high energy, high angle, etc.) of the grain boundaries has a stark affect on the presence of midband-gap states within the material, which are strongly affected by the deposition conditions. Since we varied the substrate temperature during growth of the NCD films, we anticipate variations in grain size and grain boundaries, which are reflected in the volume fraction of trigonal (sp^2-C) and tetrahedral (sp^3-C) bonded carbon in the films, since most of the observed sp^2-C in CVD diamond films is seen at the grain boundaries.[14] The sp^2-C and sp^3-C volume fractions are qualitatively reflected in micro-Raman spectra of the films (not shown), in which s@800 showed narrow *D* and *G* bands, where as s@600 and s@400 illustrated broad band's typical of NCD films. Also, the XPS carbon 1*s* core-loss spectroscopy[21] of s@800 showed features due to both diamond and graphitic plasmons indicating the higher graphitic nature of the film resulting in diminished TEED signal. The core-loss spectra from s@600 and s@400 films showed both surface and bulk diamond plasmon features revealing higher diamond nature. The average grain size estimated from atomic force microscopy (not shown) is ~15–20 nm and ~10 nm for s@600 and s@400 films, respectively.

We believe that the midband-gap states are most probably introduced by defects but also cannot rule out the possibility of nanometer sized grain boundary carbon. Spectroscopic ellipsometry studies[18] reported previously on a sample bombarded with the electron during the deposition, as in the present case, revealed the presence of midband-gap states. Consequently, the sp^2-C volume fraction increased through defect states within the electronic band gap. Also recent electron paramagnetic resonance and nuclear magnetic resonance studies on ultra-NCD (UNCD) films with nanometer sized grain boundaries revealed structural defects at the interface between grain and the detached graphene layers that cover diamond grain and also sp^3 diamondlike defects (dangling bonds).[44] This connects to the origin behind the consistent thermionic emission from s@600 and s@400 NCD films by midband-gap states probably introduced as a result of structural defects at the nanometer sized grain boundary leading to the low work function of approximately 3.3 eV. The existence of a midband-gap state is further supported by an experimentally examined 3.2 eV state in NCD films by Yoneda *et al.*[45] using time-resolved reflectance measurements. We note that nanometer sized grain boundaries, are also the source of field emitted electrons and field enhancement in UNCD films.[21]

Focusing our attention on the mechanism, electron emission from the films has at least three important components: (i) injection of electrons from substrate to the film, (ii) transport through the film, and (iii) ejection from the surface. Here, we focus on the third and second components. Though the electron emission from NCD films for both field and thermionic emission may originate from nanometer sized grain boundaries there is fundamental difference in the mechanism. The contribution to field emission comes from narrow energy bands close to the Fermi level,[46] which upon the application of field (field enhancement at diamond-grain boundary-vacuum interface) reduce the barrier width for electron tunneling, whereas the thermionic emission contribution comes from energy bands close to the top of the potential barrier (for semiconductors that will be energy states close to conduction band)[46] and the electrons overcome the barrier thermally. Since there is no large external applied field, the emission from the s@600 and s@400 films is thermionic and TEEDs suggest that the electrons overcome the potential barrier relatively easily from the midband-gap energy states (close to VL) created by the structural defects at the nanometer sized grain boundaries. Addressing the second component, transport through the NCD films, detailed computational studies were done by Cleri *et al.*[47] and Keblinski *et al.*,[43] suggested hopping conduction through localized π^* states by sp^2 bonded carbon in sufficiently dense and connected high-energy grain boundaries, as should be the case of NCD. Hence, the origin and mechanism of the consistent low work function peak at 3.3 eV are elucidated.

IV. CONCLUSIONS

TEEDs measured from NCD films deposited under positive bias conditions (electron bombardment) using Ar-rich HFCVD revealed a consistent low work function of approximately 3.3 eV over the temperature range of 700–900 °C. The s@600 NCD exhibited this emission peak even after heating to maximum temperature of 900 °C, although heating the s@400 NCD to above 850 °C permanently eliminated the emission peak near 3.3 eV. The origin of this low work function in the NCD films is discussed using energy level band motive diagram for different operative phenomena including NEA, Fermi level pinning, and midband-gap states. The analysis suggests that the observed low work function in NCD is probably due to midband-gap states introduced as a result of structural defects at the nanometer sized grain boundaries. These midband-gap states are consistent with previous work using spectroscopic ellipsometry. The finding of a thermally stable reduced work function state permits some optimism for the realization of low-temperature direct thermionic energy conversion devices using NCD films.

ACKNOWLEDGMENTS

The author K.U. acknowledges the financial support provided by the fellowship (National Science Foundation under Grant No. EPS-0223152) for the internship at Birck Nanotechnology Centre (Purdue University, West Lafayette). This research project is being carried out under the auspices of the Institute for Functional Nanomaterials (NSF Grant No. 0701525).

[1]G. Hatsopoulos and E. Gyftopoulos, *Thermionic Energy Conversion* (MIT Press, Cambridge, MA, 1973), Vol. 1.
[2]G. Hatsopoulos and E. Gyftopoulos, *Thermionic Energy Conversion* (MIT Press, Cambridge, MA, 1973), Vol. 2.
[3]V. S. Robinson, Y. Show, G. M. Swain, R. G. Reifenberger, and T. S. Fisher, Diamond Relat. Mater. **15**, 1601 (2006).
[4]A. Shakouri, Z. Bian, R. Singh, Y. Zhang, D. Vashaee, T. E. Humphrey, H. Schmidt, J. M. Zide, G. Zeng, J-H. Bahk, A. C. Gossard, J. E. Bowers, V. Rawat, T. D. Sands, W. Kim, S. Singer, A. Majumdar, P. M. Meyer, R. J. Ram, K. J. Russel, V. Narayanamurti, F. A. M. Koeck, X. Li, J.-S. Park, J. R. Smith, G. L. Bilbro, R. F. Davis, Z. Sitar, and R. J. Nemanich, Mater. Res. Soc. Symp. Proc. **886**, 0886-F07001.1 (2006).
[5]H. Oman, IEEE Aerosp. Electron. Syst. Mag. **18**, 28 (2003).
[6]T. S. Fisher and D. G. Walker, ASME J. Heat Transfer **124**, 954 (2002).
[7]F. A. M. Kock, J. M. Garguilo, and R. J. Nemanich, Diamond Relat. Mater. **10**, 1714 (2001).
[8]J. M. Garguilo, F. A. M. Koeck, R. J. Nemanich, X. C. Xiao, J. A. Carlisle, and O. Auciello, Phys. Rev. B **72**, 165404 (2005).
[9]V. S. Robinson, T. S. Fisher, J. A. Michel, and C. M. Lukehart, Appl. Phys. Lett. **87**, 061501 (2005).
[10]J. Li, V. S. Robinson, Y. Liu, W. Lu, T. S. Fisher, and C. M. Lukehart, Nanotechnology **18**, 325606 (2007).
[11]T. L. Westover, A. Dighe, P. Amama, and N. Lilovich, Proceedings of the Second Energy Nanotechnology International Conference, Santa Clara, CA, 2007 (unpublished), p. 45043.
[12]F. A. M. Koeck and R. J. Nemanich, Diamond Relat. Mater. **15**, 217 (2006).
[13]F. A. M. Koeck and R. J. Nemanich, Diamond Relat. Mater. **14**, 2051 (2005).
[14]D. M. Gruen, Annu. Rev. Mater. Sci. **29**, 211 (1999).
[15]L. C. Qin, D. Zhou, A. R. Krauss, and D. M. Gruen, Nanostruct. Mater. **10**, 649 (1998).
[16]A. R. Krauss, O. Auciello, M. Q. Ding, D. M. Gruen, Y. Huang, V. V. Zhirnov, E. I. Givargizov, A. Breskin, R. Chechen, E. Shefer, V. Konov, S. Pimenov, A. Karabutov, A. Rakhimov, and N. Suetin, J. Appl. Phys. **89**, 2958 (2001).
[17]A. Erdemir, C. Bindal, G. R. Fenske, C. Zuiker, A. R. Krauss, and D. M. Gruen, Diamond Relat. Mater. **5**, 923 (1996).
[18]S. Gupta, B. R. Weiner, and G. Morell, Diamond Relat. Mater. **10**, 1968 (2001).
[19]K. Uppireddi, B. R. Weiner, and G. Morell, Diamond Relat. Mater. **17**, 55 (2008).
[20]K. Uppireddi, Ph.D. thesis, University of Puerto Rico, 2008.
[21]K. Uppireddi, B. R. Weiner, and G. Morell, J. Appl. Phys. **103**, 104315 (2008).
[22]J. W. Gadzuk and E. W. Plummer, Rev. Mod. Phys. **45**, 487 (1973).
[23]R. D. Young and C. E. Kuyatt, Rev. Sci. Instrum. **39**, 1477 (1968).
[24]R. Reifenberger, H. A. Goldberg, and M. J. G. Lee, Surf. Sci. **83**, 599 (1979).
[25]V. S. Robinson, M.A. thesis, Purdue University, 2005.
[26]T. L. Westover, Ph.D. thesis, Purdue University, 2008.
[27]A. A. Brown, L. J. Neelands, and H. E. Farnsworth, J. Appl. Phys. **21**, 1 (1950).
[28]M. H. Nichols, Phys. Rev. **57**, 297 (1940).
[29]H. Kawarada, Surf. Sci. **165**, 83 (1996).
[30]J. B. Cui, J. Ristein, M. Stammler, K. Janischowsky, G. Kelber, and L. Ley, Diamond Relat. Mater. **9**, 1143 (2000).
[31]F. A. M. Köck, J. M. Garguilo, B. Brown, and R. J. Nemanich, Diamond Relat. Mater. **11**, 774 (2002).
[32]F. A. M. Koeck, J. M. Garguilo, and R. J. Nemanich, Diamond Relat. Mater. **13**, 2052 (2004).
[33]O. Gröning, O. M. Küttel, P. Gröning, and L. Schlapbach, J. Vac. Sci. Technol. B **17**, 1970 (1999).
[34]D. Takeuchi, H. Kato, G. S. Ri, T. Yamada, P. R. Vinod, D. Hwang, C. E. Nebel, H. Okushi, and S. Yamasaki, Appl. Phys. Lett. **86**, 152103 (2005).
[35]B. M. Nichols, J. E. Butler, J. N. Russell, Jr., and R. J. Hamers, J. Phys. Chem. B **109**, 20938 (2005).
[36]J. B. Cui, J. Ristein, and L. Ley, Phys. Rev. Lett. **81**, 429 (1998).
[37]J. Van der Weide, Z. Zhang, P. K. Baumann, M. G. Wensell, J. Bernholc, and R. J. Nemanich, Phys. Rev. B **50**, 5803 (1994).
[38]Y. V. Pleskov, M. D. Krotova, V. V. Elkin, V. G. Ralchenko, A. V. Khomich, and R. A. Khmelnitskiy, Electrochim. Acta **50**, 1149 (2005).
[39]S. Bhattacharyya, Phys. Rev. B **70**, 125412 (2004).
[40]P. Zapol, M. Sternberg, L. A. Curtiss, T. Frauenheim, and D. M. Gruen, Phys. Rev. B **65**, 045403 (2001).
[41]A. Llie, A. C. Ferrari, T. Yagi, and J. Robertson, Appl. Phys. Lett. **76**, 2627 (2000).
[42]P. Keblinski, D. Wolf, F. Cleri, S. R. Phillpot, and H. Gleiter, MRS Bull. **23**, 36 (1998).
[43]P. Keblinski, D. Wolf, F. Cleri, S. R. Phillpot, and H. Gleiter, J. Mater. Res. **13**, 2077 (1998).
[44]A. I. Shames, A. M. Panich, S. Porro, M. Rovere, S. Musso, A. Tagliaferro, M. V. Baidakova, V. Yu. Osipov, A. Ya. Vul, T. Enoki, M. Takahashi, E. Osawa, O. A. Williams, P. Bruno, and D. M. Gruen, Diamond Relat. Mater. **16**, 1806 (2007).
[45]H. Yoneda, K. Tokuyama, R. Yamazaki, K. Ueda, H. Yamamoto, and K. Baba, Appl. Phys. Lett. **77**, 1425 (2000).
[46]A. Modinos, *Field, Thermionic, and Secondary Electron Emission Spectroscopy* (Plenum, New York, 1984).
[47]F. Cleri, P. Keblinski, L. Colombo, D. Wolf, and S. R. Phillpot, Europhys. Lett. **46**, 671 (1999).